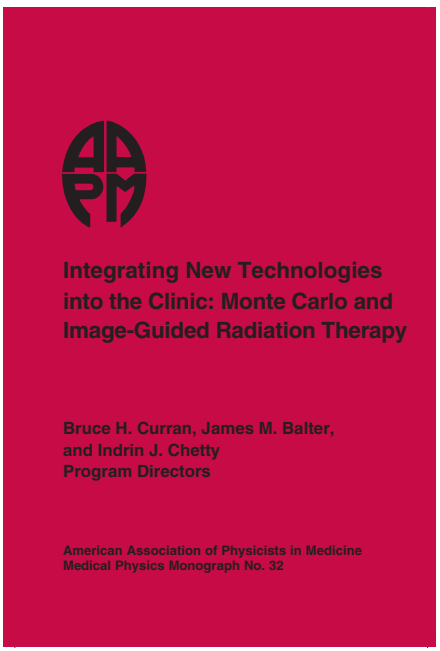

Here is a sample chapter from this book.

Monte Carlo Applications in IMRT Planning and Quality Assurance

Jeffrey V. Siebers, Ph.D.[1] and C.-M. Charlie Ma, Ph.D.[2]
[1]Department of Radiation Oncology
Virginia Commonwealth University, Richmond, Virginia
[2]Radiation Oncology Department
Fox Chase Cancer Center, Philadelphia, Pennsylvania

Introduction

This chapter covers the role of Monte Carlo (MC) dose-computation algorithms in intensity modulated radiation therapy (IMRT) quality assurance (QA) and treatment-plan optimization. To date, MC has been used to validate IMRT planning programs, to perform patient-specific IMRT QA, and to optimize both photon-beam and electron-beam IMRT plans (Jeraj and Keall 1999; Ma et al. 1999; Laub et al. 2000; Li et al. 2000, 2004; Ma et al. 2000a,b, 2003a,b, 2004; Deng et al. 2001; Keall et al. 2001;

Lee et al. 2001; Pawlicki and Ma 2001; Lee 2002; Wang, Yorke, and Chui 2002; Alber et al. 2003; Leal et al. 2003; Ma et al. 2003a,b; Siebers and Mohan 2003; Heath, Seuntjens, and Sheikh-Bagheri 2004; Pawlicki et al. 2004; Xiong et al. 2004; Boudreau et al. 2005; Yang et al. 2005). Although MC is not yet in widespread routine clinical use for IMRT dose evaluation or treatment-plan optimization, the knowledge gained from the work completed thus far on this topic can aid physicists and clinicians in understanding limitations in the accuracy of IMRT dose algorithms, the sources of dose inaccuracies, and their impact on plan optimization and provide a basis for improving the IMRT process. The purpose of this chapter is to educate the reader as to:

1. The methods used to incorporate MC into the IMRT dose-calculation process, including a discussion of the trade-offs between the various methods.

2. The role of MC in general treatment-planning system (TPS) IMRT QA, including a general discussion on the sources of dose inaccuracies in non-MC dose algorithms.

3. The role of MC in performing patient-specific IMRT QA, including QA processes that can be implemented in centers that have MC dose-computation capabilities.

4. The use of MC in photon-beam IMRT optimization, including a discussion of methods that may make this clinically realizable within a few hours of dose-computation time.

5. The use of MC in energy and intensity-modulated electron-beam radiation therapy (MERT) optimization.

6. The possible future roles of MC in per-treatment IMRT QA, including using MC in conjunction with multileaf collimator (MLC) leaf log files to aid in reconstructing patient-dose delivery and the use of MC to accurately compute electronic portal imaging device (EPID) portal images for the beam delivery through the patient treatment volume.

Monte Carlo Dose-Calculation Methods for IMRT

In this section, the general methods used to incorporate MC into IMRT dose calculation are described. This is done to provide a general understanding of the levels at which MC can be integrated into the dose computation, since the extent to which MC is integrated into the dose-calculation process will dictate the ability of MC to improve dose evaluation. In general, the radiation therapy dose-calculation process can be considered to consist of two processes:

1. Determining the fluence of radiation incident upon the volume of interest (the patient or the phantom).

2. Determining the energy deposition resulting from that incident energy fluence within the volume of interest.

Monte Carlo dose-calculation methods can be used for both of these processes, or, in some instances, for only one of these processes. Consequently, the discussion below first subdivides MC dose-calculation methods into the two categories listed above, followed by presentation of how these processes can be combined with each other and with other dose-computation processes to compute patient-dose distributions.

MC for Intensity-Modulated Incident Fluence Prediction

IMRT differs from three-dimensional conformal radiation therapy (3DCRT) in that 3DCRT utilizes multiple beams with uniform open-field radiation fluences, truncated by an aperture edge to achieve a desired dose distribution, while in IMRT, for each beam direction, the radiation fluence incident upon the patient is modulated so as to achieve a desired dose distribution within the patient. For most IMRT treatments, the fluence ("intensity") modulation is achieved via use of an MLC. The two major paradigms used for IMRT delivery (Boyer et al. 2001) are multisegmented IMRT (also called step-and-shoot IMRT) and dynamic MLC-based IMRT. The former is termed *SMLC* and the latter is termed *DMLC* for the remainder of this chapter. For details on IMRT delivery, the interested reader is referred to the 2003 AAPM Summer School proceedings (Mackie and Palta 2003). Note, other forms of IMRT delivery exist, including the use of compensators, the TomoTherapy™ delivery device, and intensity-modulated arch therapy (IMAT), to name a few. While this chapter will concentrate on cone-beam delivery-based SMLC and DMLC IMRT delivery, the concepts presented here can generally be extended to these other IMRT delivery paradigms.

MC MLC Modeling

A prerequisite to using MC to predict the incident fluence prediction is some type of MC geometric and radiation transport model for the MLC. For an ideal MLC, no radiation is transmitted through the MLC, making even rudimentary transport algorithms sufficient. For realistic MLCs, ~2% of the incident radiation is transmitted by the MLC. Thus, for IMRT fields, where monitor units can be up to five times those of a 3DCRT field, MLC-transmitted radiation can account for ~10% of the dose received by the patient, with additional components due to transmission through MLC leaf tips (Mohan et al. 2000). For some structures, nearly all of the radiation dose delivered can be attributed to radiation transmitted through the MLC leaves. Thus, accurate modeling of the MLC may be important to ensure accurate patient-dose evaluation.

There are numerous published algorithms for modeling the MLC for MC IMRT dose calculations. Using the modules described below, for SMLC IMRT delivery, MC

simulations can be performed for each segment of the beam delivery with the number of source particles transported per segment being proportional to the monitor units (MUs) delivered through the segment. For DMLC IMRT, either explicit motion of the MLC must be included in the sampling routine (Siebers et al. 2002b; Lui, Verhaegen, and Dong 2001), or a large number of static fields (hundreds) or static segments must be included to simulate the dynamic delivery (Fix et al. 2001).

General-purpose MC algorithms. General-purpose MC codes, such as MCNP (Briesmeister 2000) or GEANT (CERN Application Software Group and Computing and Network Division 1995) can be used to model radiation transmission through MLCs. MCNP allows complete modeling of all of the geometric details of the MLC via use of its combinatorial geometry package (Kim et al. 2001); however, the overhead associated with transporting particles through the geometry results in a process that is too slow for clinical-type dose computations. [For MCNP, it is estimated that ~50 hours would be required on 2-GHz processors to transport enough particles for sufficient statistical precision (2%) through the full MLC geometry.] The general-purpose MC codes are most useful for investigating generic features of MLC-transmitted radiation, such as differences between the photon-energy spectra in an open field and that transmitted by the MLC, the radiation subcomponents of radiation leakage, and the contributions of radiation leakage as a function of field size (Fix et al. 2001; Kim et al. 2001). The general applicability of the general-purpose MC code to simulate patient field IMRT fluence prediction was demonstrated by Fix et al. (2001), who used GEANT to simulate phantom-based IMRT film QA measurements and showed agreement with film measurements for a single field to within 2.5% and 1.5 mm. However, these simulations were very time consuming, requiring >100 hours of CPU (central processing unit) time to simulate the IMRT field.

BEAM/EGS component modules. A large number of MC component modules have been written for the user codes BEAM (Rogers et al. 1995) and BEAMnrc (Rogers et al. 2001), which use EGS4 (Nelson, Hirayama, and Rogers 1985) and EGSnrc (Kawrakow 2000), respectively. The current BEAMnrc manual lists five component modules for MLCs:

> **MLC:** Models a generic double-focusing MLC with flat faces. Since this model has flat edges, it does not allow modeling of tongue-and-groove effects.
>
> **MLCQ:** Models a single-focused MLC that has rounded leaf ends (MLCQ) (De Vlamynck et al. 1999), and does not model the tongue-and-groove leaf design.
>
> **VARMLC:** Models a single-focused MLC that has rounded leaf ends and includes a tongue-and-groove leaf design similar to that of the 80-leaf Varian MLC, including air gaps between adjacent leaves (Kapur, Ma, and Boyer 2000).
>
> **DYNVMLC:** A variant of VARMLC, which is designed specifically for modeling the 120-leaf Varian Millennium MLC (Heath and Seuntjens 2003).

MLCE: Models Elekta MLCs, including their tongue-and-groove leaf design (Van de Wallw et al. 2003).

These MLC modules allow for full simulation of radiation interactions within the MLC, although the geometry varies from simple to complex. A similar feature of all of the BEAMnrc MLC modules is the relatively large amount of time required to complete an IMRT-type simulation, which would typically require tens to hundreds of hours if the simulation were to be performed on a single CPU. This excessive computation time limits the routine clinical application of such modules for IMRT optimization or plan verification.

The Peregrine MLC module. The Peregrine MC program is reported to include explicit transport through the MLC leaves, including rounded leaf ends and tongue-and-groove features (Hartmann Siantar et al. 2001). For Varian leaf designs, Peregrine doses were reported to agree with measured test fields within 2% after adjustments were made (Heath, Seuntjens, and Sheikh-Bagheri 2004), although discrepancies that result in ~10% dose errors to critical structures have been reported for Elekta MLCs (Reynaert et al. 2005).

Independent MC MLC modules. Specialized MC MLC modules designed specifically for IMRT have been developed with the intent of reducing the overall calculation time to clinically acceptable levels, while not introducing clinically unacceptable bias into the MC simulation result (Keall et al. 2001; Siebers et al. 2002a). The model of Siebers et al. simplified the problem by (a) ignoring electron transport within the MLC, (b) only including first Compton events in the MLC scatter radiation, and (c) simplifying the transport through the complex MLC geometry for highly divergent particles that are likely to miss the patient plane. In addition to the physics and geometry approximations, the photon efficiency was improved by determining the photon-attenuation probability for multiple (100) random time segments during the delivery and by modifying the incident beam weight by the average probability of the photon surviving through the MLC. This simple technique avoids wasting time on sourcing particles that are unable to interact in the patient since they are attenuated in the MLC. To avoid the transport of low relative weight photons in the patient, exiting photons can be processed with a Russian roulette variance reduction scheme. Overall, the model simplifications allowed a several hundred-fold speed increase in comparison with general-purpose MC algorithms, yet reproduced measurements within ±1% or ±1 mm for both 6-MV and 18-MV test cases. To run sufficient particles to compute the dose to 2% statistics in 4-mm cubic voxels for a typical prostate IMRT field, less than 2 minutes is required for the MLC transport.

An important conclusion of the benchmarks with the independent MLC module is that neglecting electron transport in the MLC does not introduce substantial bias in the patient dose computation,[1] thus enabling similar approximations to be made in

[1] The lack of MLC electrons results in a ~5% underprediction of the dose at the phantom surface, however, this corresponds to a <1.0-mm distance to dose agreement at the surface.

other MLC modules. Simple experiments indicate that this can result in a speed enhancement of five or more for the BEAM component modules.

MC for Prediction of Dose in Patient Volumes

Motivation

A principal advantage of MC dose-computation algorithms is their ability to accurately compute dose for arbitrarily complex fluence patterns in arbitrarily complex geometric media. Unlike many conventional algorithms (non-MC), MC makes no assumptions regarding radiation equilibrium conditions; thus, MC algorithms can accurately compute dose for both small field sizes and for heterogeneous patient geometries, such as those found for head-and-neck and lung patients. Inaccuracies in conventional algorithms are most apparent for small treatment fields, particularly when traversing tissue heterogeneities (Ma et al. 1999; Arnfield et al. 2000; Jones, Das, and Jones 2003; Jones and Das 2005). An example of this is shown in Figure 1, which compares algorithms for a 4×4 cm^2 6-MV field incident on a water phantom that has a 2-cm air cavity inserted between the depths of 3 cm and 5 cm. Even for this relatively large field size, only MC accurately reproduces the measured (a) depth dose and the (b) lateral profile at the distal interface. For a more clinically relevant 0.26 g/cm^3 lung heterogeneity (Figure 2), the error with non-MC algorithms is small for a 3-cm diameter field size. For IMRT beamlet-sized dose distributions with 1.0-cm and 0.5-cm diameters, differences between MC and convolution techniques persist (Jones and Das 2005). For IMRT fields, differences between MC and conventional algorithms depend upon the incident fluence modulation directed toward the dose region of interest. In large uniform fluence regions within IMRT fields, differences should be similar to those for 3DCRT beams of similar field sizes. In highly modulated regions, on the other hand, differences characteristic of small fields will be proportionally superimposed on the field produced by the uniform fluence background.

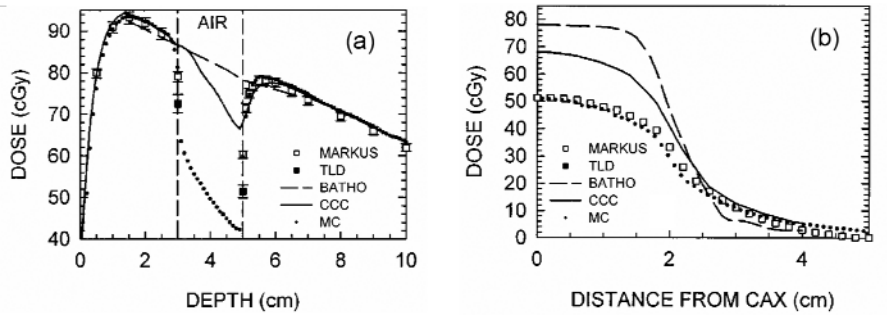

Figure 1. Depth-dose (a) and lateral profile (b) comparisons between measurement, Monte Carlo (MC), collapsed-cone convolution (CCC), and a radiological path-length BATHO algorithm for a 4×4 cm^2 6-MV field incident on a phantom containing water and air.

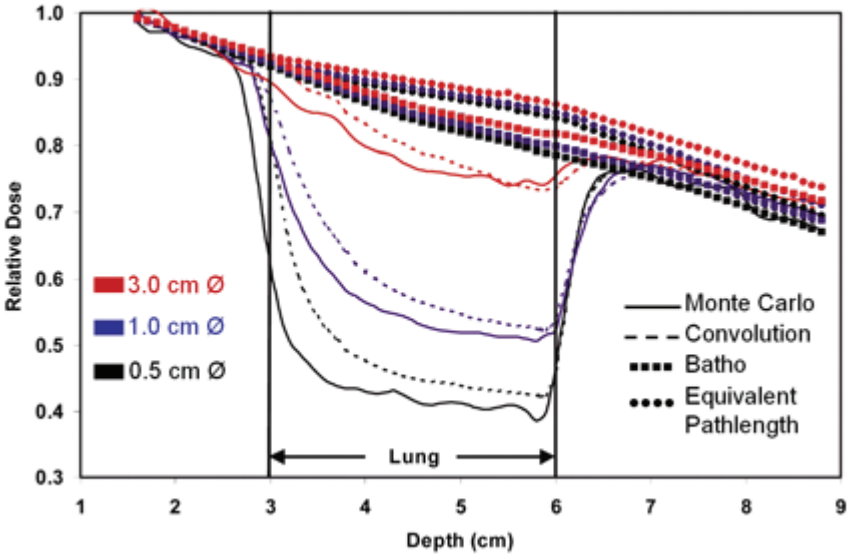

Figure 2. Field-size dependence of the heterogeneity failure of conventional dose algorithms for a water phantom with a 3-cm thick 0.26 g/cm^3 lung insert with a 6-MV photon beam incident. (Adapted from *Med Phys*, vol 32, "Comparison of inhomogeneity correction algorithms in small photon fields," A. O. Jones and I. J. Das. pp. 766–776. © 2005, with permission from AAPM.)

Bixel-based Dose Computation

One method to compute IMRT patient dose distributions is to utilize a method termed *bixel*-based dose computations. In bixel-based dose computations, the beam's-eye-view projection of each treatment beam (each with a different gantry, couch, or collimator angle) is subdivided into rectangular beam-intensity elements. Typically, each beam intensity element is 1×1 cm^2 at 100 cm source-to-axis distance (SAD).[2] The dose resulting from the fluence delivered through each individual beam element is then computed with either an MC algorithm or another dose-computation algorithm and stored for use during plan optimization. The dose distribution from a single beam-intensity element is termed a *bixel*. Due to their relatively coarse resolution, bixel-based IMRT dose computations and optimizations are usually associated with SMLC IMRT delivery.

The advantage of using bixels for IMRT dose computation is that each bixel only needs to be computed once for a given patient geometry. The IMRT optimization

[2] Fluence resolution is limited by the memory required to store the associated 3-D dose grid elements. For each intensity element, the 3-D dose distribution from that intensity element must be saved.

process determines the weighting of the individual bixels required to produce the desired dose distribution.

Apart from the limited resolution of the bixels, the major disadvantage of the bixel method is that the incident radiation fluence used in the bixel dose computation inherently ignores the detailed aspects of the beam delivery. As a result, the effects of MLC leakage and scatter radiation, particularly the component that is partially transmitted through the MLC leaf tips (in the case of rounded leaf ends), are ignored. Although it has not been studied in detail, logically, this approximation will depend upon the size of the bixels used during optimization (smaller bixels, larger MLC effects). Note that following bixel-based dose computations with computations that directly simulate through the leaf sequences required to deliver the bixels can mitigate the impact of MLC leakage-induced errors.

Field-based Dose Computation

The most common method of using MC to compute IMRT dose distributions is to compute the 3D patient dose distribution for some (modulated) integral incident fluence. This method is termed *field-based dose* (*FBD*) computation here for clarity. MC methods to achieve the fluence modulation were presented previously, but other methods can be used as well as described below. Advantages of the FBD method include the fact that fluences directly from MC simulations, which include the details of the full treatment head (including the MLC), can be used as input. Therefore, the full effects of MLC scatter and beam hardening on the IMRT dose distribution can be included in the patient dose evaluation. For SMLC IMRT delivery, the FBD method can be used to compute individual beam-delivery segments, which can then be used in deliverable segment-based plan re-optimization. A disadvantage of the FBD computation is that dose computation must be performed each time the fluence segments change (MLC leaf positions change). For DMLC-based IMRT delivery, this requires dose re-computation for each IMRT optimization iteration, which can result in multiple MC simulations through the patient anatomy.

Combining Fluence Prediction and Patient Dose

With the dose-computation process separated into two components, it is easy to see that MC can be used for either one or both parts of the dose-computation processes. Permutations used include the following.

Analytic Fluence with MC Patient Dose Algorithms

Fluences (or fluence-weighting factors) derived from non-MC algorithms can be used as input to IMRT MC patient dose evaluations. In this case, the fluence intensity modulation is estimated by using the intensity modulation specified by the TPS or via independently generated fluence-modulation matrices or beamlet weighting factors. When the patient-specific MC simulation is performed, instead of transporting the

particle through the MLC, the statistical weight particle is reduced by the effective MLC transmission. That is, a particle with statistical weight w_i with coordinates (x,y) is modified so its final weight w_f is

$$w_f(x,y) = w_i(x,y) \times T(x,y), \tag{1}$$

where $T(x,y)$ is the fluence transmission.

Since the MC method simulates the radiation transport through the patient, this method accounts for the effects of patient heterogeneities on the dose. However, because this method neglects potential errors in fluence prediction, the final result is only as accurate as the external fluence prediction method. Bixel-based dose computations (without the corresponding MLC leaf sequences) fall into this class of algorithm, as do the methods that use the TPS intensity matrix (Wang, Yorke, and Chui 2002) and methods that use intensity matrices generated independently of the treatment-planning program, (Ma et al. 2000a; Pawlicki and Ma 2001; Aaronson et al. 2002).

MC Fluence with MC Patient Dose Calculations

The most rigorous method of including MC in the dose-computation process is to model both the fluence delivery and the patient dose deposition using MC methods, since then the effects of MLC leakage and scatter are fully incorporated into the dose computation, as are the detailed effects of particle transport through patient heterogeneities. In practice, for SMLC, this can be accomplished by computing patient dose distributions from each individual SMLC segment and then by summing the weighted dose distributions. For DMLC, the MLC leaf sequence can be treated as either continuously moving during the beam delivery or as subdivided into a large number of static segments.

MC Fluence with Analytic Patient Dose Algorithm

The final possible permutation is to combine MC-derived fluence estimates with analytic patient dose algorithms. This technique has merits, as IMRT QA done on homogeneous phantoms often shows dose discrepancies, indicating that fluence prediction may be the downfall of the (analytic) dose-calculation algorithms.

To incorporate intensity modulation, analytic dose-computation algorithms require an energy fluence transmission matrix (T) with which the incident energy fluence $\psi_0(x,y)$ is multiplied to get the energy fluence exiting the MLC and incident upon the patient

$$\psi_{MLC}\left(x,y\right) = T(x,y) \times \psi_0\left(x,y\right). \tag{2}$$

Generating the T matrix with MC requires simulating particles from the source to the plane containing the T matrix (typically isocenter) twice, once for an open field, neglecting the effect of fluence modulation, and once for the MLC-modulated field. The energy fluence ($E_i \times w_i$, where E_i is the energy of the particle, and w_i is the statistical weight of the i^{th} particle) is scored into $\psi_0(x,y)$ and $\psi_{MLC}(x,y)$ on a particle-by-particle basis for the open and MLC-modulated fields, respectively. The ratio of the open-field and MLC-modulated energy fluence values allows simple determination of $T(x,y)$.

$$T(x,y) = \frac{\psi_{MLC}\left(x,y\right)}{\psi_0\left(x,y\right)} \quad \forall \quad (x,y) \ . \tag{3}$$

Note that T accounts for the radiation transmitted through and scattered from the MLC leaves, as well as inter- and intraleaf leakage. However, since the fluence matrix amalgamates the energy fluence on a plane, differential beam hardening (Fix et al. 2001; Kim et al. 2001) and the directional dependence of the scattered radiation are lost. These are inherent limitations of the transmission matrix approach with respect to the MC particle-by-particle simulation approach.

MC for IMRT QA

The use of IMRT techniques is a major departure from the way radiotherapy has traditionally been delivered. Although the use of MLC provides the possibility of achieving better dose distributions conformed to tumor targets, it also increases the treatment complexity. The sequences of leaf movement and their associated effects on the dose delivered to the patient may vary significantly, depending on the accelerator and the MLC design. Important factors include the variation of the accelerator head scatter component in the MLC-collimated beam (Brahme 1988; Convery and Rosenbloom 1992; Boyer and Strait 1997), the amount of photon leakage through the leaves (Wang et al. 1996; Webb 1997), the scatter from the leaf ends, the "tongue-and-groove" effect (Chui, LoSasso, and Spirou 1994; Wang et al. 1996; Deng et al. 2001), and the effect of back-scattered photons from the moving jaws and MLC leaves on the monitor chamber signal (Hounsell 1998; Verhaegen et al. 2000; Jiang, Boyer, and Ma 2001). Furthermore, most inverse-planning algorithms for beam optimization have used approximations to speed up the dose computation, which may introduce significant uncertainty in the calculated dose distributions, especially in the presence of heterogeneities. When simple source models are used in the dose computation, the correlation between the calibrated reference dose and the dose related to a beam segment may be lost. All of the above imply a potential problem with the prediction of the dose distributions in a patient for an IMRT treatment. Monte Carlo simulations have played an important role in the IMRT QA process.

TPS Verification

Several investigators have reported their dosimetric verification of the TPSs used for IMRT treatment optimization (Ma et al. 1999, 2000a; Arnfield et al. 2000; Pawlicki and Ma 2001; Jeraj, Keall, and Siebers 2002; Siebers and Mohan 2003; Yang et al. 2005). Ma et al. (2000a) used Monte Carlo simulations to verify the accuracy of the dose distributions from a commercial treatment-planning optimization system for IMRT. They modified a previously implemented MC dose-calculation system to recompute the dose in a patient for multiple-beam, fixed-gantry IMRT treatments. The information in the linear accelerator MLC leaf-sequence file was used to derive a fluence map from which particles were sampled during the simulations. The MLC leakage was incorporated by reducing the particle weight for the MLC-blocked sections. The dose distributions predicted by the commercial TPS agreed with the MC simulations and measurements to within 4% in a cylindrical water phantom with various hypothetical target shapes. Discrepancies of more than 5% (relative to the prescribed target dose) in the target region and over 20% in the critical structures were found in some IMRT patient calculations (Ma et al. 2000a; Pawlicki and Ma 2001). A more classical example of heterogeneous geometry is shown in Figure 3, where a patient with a reconstructed vertebral column of titanium rods was treated with eight coplanar 4-MV photon IMRT fields. The target volume included part of the lung and was also partially shielded by the titanium rods along the spinal cord. In this case, the target dose was significantly overestimated since the finite size pencil beam (FSPB) algorithm could not predict the loss of electron equilibrium at the tissue-lung interfaces. The MC dose distributions showed a large cold spot and also reduced the dose to the cord, due to the shielding effect of the titanium rods (Pawlicki and Ma 2001).

To validate the IMRT dose distributions by both the MC system and the TPS, a QA phantom that consists of a PMMA cylinder with bone and lung inserts was developed (Figure 4a) (Ma et al, 2003b). The phantom was CT scanned, and dummy targets and critical structures were contoured so that treatment plans could be generated using the TPS (Figure 4b). The plans using 4- and 15-MV photon beams were delivered on a Varian Clinac 2100C accelerator. Measurements were made at the center of the target volume using an ionization chamber, and the results were converted to dose to water following the AAPM TG-21 protocol (AAPM 1983; Ma et al. 2003b). The dose values in Table 1 were for a PMMA phantom with a central bone insert right next to the target volume. The MC calculations were carried out using the same CT data and leaf sequences as used in the phantom measurement (to reconstruct leaf leakage). The MC doses (also converted to dose-to-water) agreed well with measurements (within 1.5%), while the TPS dose was up to 5% different from the measured value for the 15-MV IMRT plan. This is a very strict test, since the phantom geometry is precisely known, and the ionization chamber measurement can be made accurately (estimated to be accurate to about 2%).

In a two-part study, Mihaylov et al. (2006) used MC IMRT dose computations to quantify IMRT dose-prediction errors. To address the potential errors introduced by

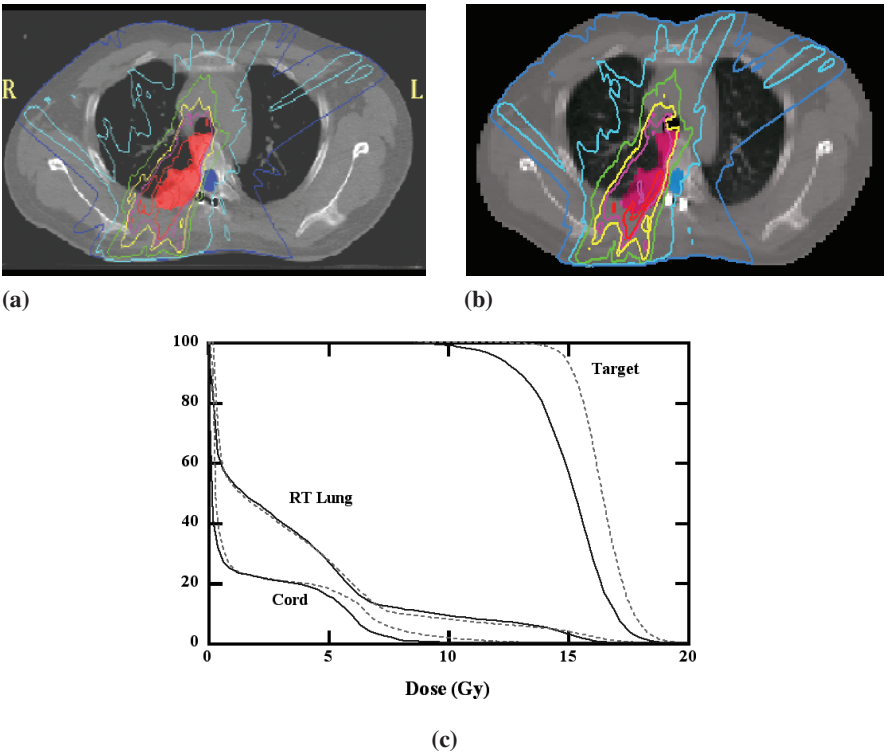

Figure 3. A patient with a reconstructed verterbral column of titanium rods was treated with eight coplanar 4-MV IMRT fields. The plans are calculated on a commercial TPS (a) and recalculated by Monte Carlo (MC) (b). The isodose values shown are 16.2, 14.4, 12.6, 9.0, 5.4, and 1.8 Gy. The DVH for the same plan (c) shows a large difference in target coverage between the TPS and MC. The solid line denotes the MC dose calculation result and the dashed line denotes the conventional dose calculation result. (Adapted from *Med Dosim*, vol 26, "Monte Carlo simulation for MLC-based intensity-modulated radiotherapy," T. Pawlicki and C.-M. Ma. "Monte Carlo simulation for MLC-based intensity-modulated radiotherapy," pp. 157–168. © 2001, with permission from the American Association of Medical Dosimetrists.)

using an analytic fluence modulation matrix during MC dose computations, MC was used to generate a fluence transmission matrix T using the algorithm normally used for transport through the MLC during patient simulations. This fluence transmission matrix T was then used for patient MC dose computations and compared with patient-based MC dose computations, which included explicit transport through the MLC. Evaluated patient dose-volume indices agreed within 2.1%, indicating that analytic fluence matrices can be accurately used as a substitute for full MLC transport, so long as the fluence matrices accurately reproduce the fluence modulation.

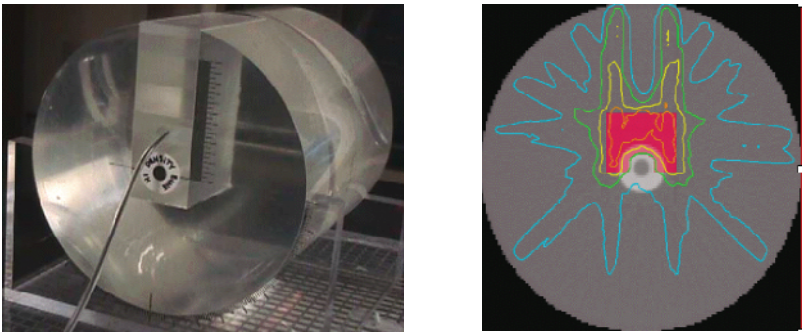

(a) **(b)**

Figure 4. A PMMA QA phantom with a central bone insert for IMRT dose verification (a), and an IMRT plan using 15-MV photon beams (b). (Adapted from *Phys Med Biol*, vol 48, "A quality assurance phantom for IMRT dose verification," C.-M. Ma, S. B. Jiang, T. Pawlicki, Y. Chen, J. S. Li, J. Deng, and A. L. Boyer, pp. 561–572.

In the second part of the study, MC was used for the fluence prediction, and the heterogeneity errors of superposition/convolution (SC) and pencil-beam (PB) algorithms were evaluated by comparing patient dose distributions with respect to those computed using MC. Figure 5 shows the ratio of the PB- and SC-computed doses with respect to MC for the dose received by 98% of the gross tumor volume (GTV) volume (GTV D_{98}) and for the parotid mean dose (D_{mean}). Statistical analysis found that although PB differs from MC by greater than 2%, no statistically significant hypothesis could be made with respect to differences between SC and MC dose algorithms. This suggests that analytic algorithms may be adequate for IMRT dose computation, particularly if they are coupled with an accurate algorithm for estimating the incident fluence.

Patient-Specific Plan Verification

Patient-specific plan verification is necessary for IMRT QA to ensure the quality of the treatment plans and the accuracy of the beam delivery (Ezzell et al. 2003). Because of the difficulty in measuring absolute dose in a patient, IMRT patient-specific QA can be generally carried out in two steps: (1) treatment-plan verification

Table 1. Comparison of IMRT Dose Values at the Center of the Target Volume

Beam Energy	Corvus	Measurement	Monte Carlo
4 MV	2.201	2.177 (1.1%)	2.177 (1.1%)
15 MV	2.276	2.161 (5.1%)	2.146 (5.7%)

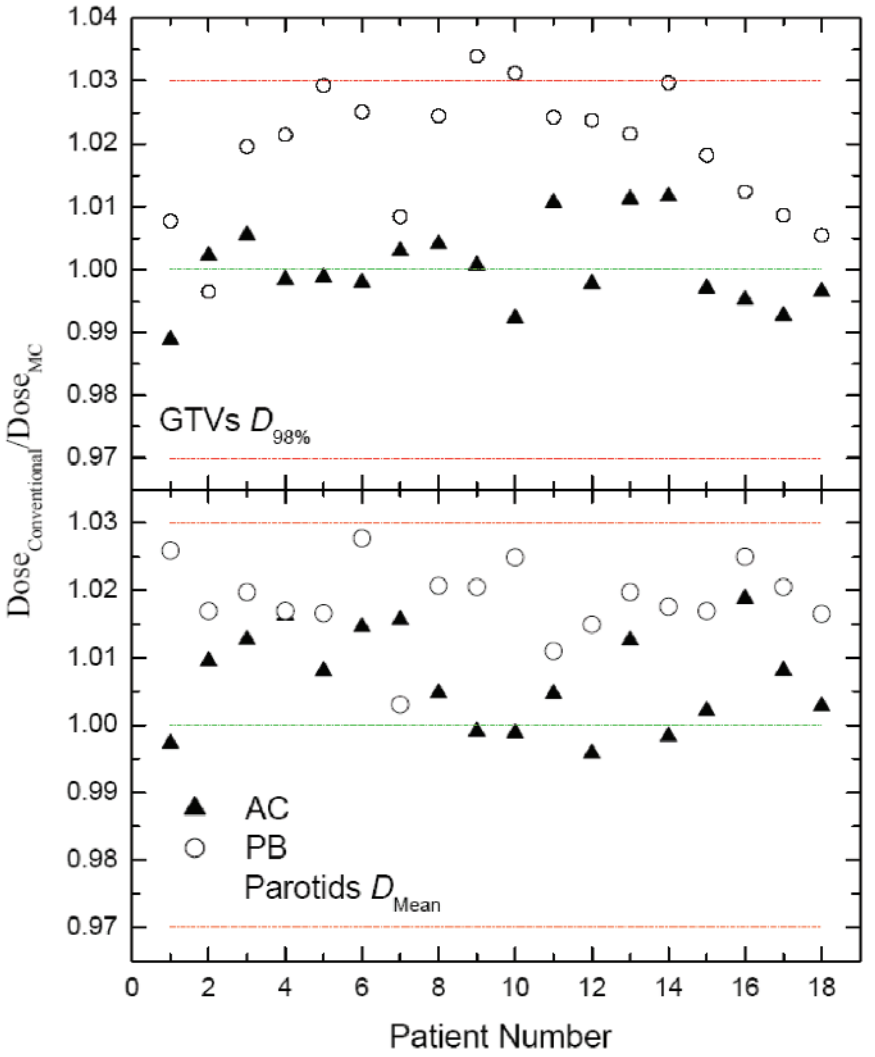

Figure 5. The dose-prediction error due to heterogeneities for PB (circles) and SC (triangles), compared with MC for 18 head-and-neck patients for the GTV D_{98} and Parotids D_{mean}. All dose-calculation methods used MC-computed fluence modulation.

and (2) beam-delivery verification. Since direct measurement is generally impossible, a different dose-calculation algorithm can verify patient dose distributions. Monte Carlo simulations are ideal for this application, and a commercial MC system has been implemented for this purpose (Heath, Seuntjens, and Sheikh-Bagheri 2004; Boudreau et al. 2005). IMRT plan verification, using home-grown MC systems, has

been reported in several academic centers (Wang et al. 1996; Ma et al. 2000a, 2003b, 2004; Keall et al. 2001; Li et al. 2001, 2004; Pawlicki and Ma 2001; Wang, Yorke, and Chui 2002; Leal et al. 2003; Siebers and Mohan 2003; Seco et al. 2005; Yang et al. 2005; Luo et al. 2006), but is not routinely done in most hospitals. Patient-specific beam-delivery QA has been carried out routinely using specially designed phantoms with ion chambers and film (Boyer et al. 1999; Ibbott et al. 2002; Ezzell et al. 2003; Ma et al. 2003b). In this process, the patient plan is delivered to a phantom and compared with the dose distributions recalculated by the TPS using the same treatment parameters and leaf sequences. Film can yield relative dose distributions in the phantom, while ion chambers can measure absolute doses. However, these measurements cannot ensure the accuracy of the patient dose distribution, since the phantom dose distribution can be significantly different from the patient dose distribution depending on the phantom geometry. Since an independent MU check is required, while the large number of MLC segments have made manual MU calculation impractical for MLC-based IMRT beam delivery, MC-based MU check tools have been investigated for patient-specific QA (Ma et al. 2004; Fan et al. 2006).

MC for IMRT Verification Using MLC Log Files and R&V Information

Conventional IMRT QA procedures using film and ion chamber measurements are useful but time consuming and limited with respect to the actual dose distributions received by the patient. Luo et al. (2006) proposed an MC-based patient-specific IMRT QA method that reconstructs the patient dose distribution using the patient CT, actual beam data based on the information from the record-and-verify system (R&V), and the MLC log files obtained during dose delivery, and that precisely records the MLC leaf positions and MUs delivered. The difference between the MC dose distribution obtained using this method and that using the leaf sequences generated by the original plan reveals the accuracy of both IMRT dose calculation, plan data transfer, and beam delivery. By combining with a routine machine/MLC QA procedure, the log-file–based MC simulation can be used as a useful and convenient patient-specific IMRT QA modality. The concept of average leaf position error was defined to analyze the MLC leaf position error for an IMRT plan. A linear correlation between the target dose error and the average position error was found, based on log-file–based MC simulations, and an average position error of 0.2 mm would lead to a target dose error of about 1.0%. This method can be used for pretreatment IMRT plan QA by irradiating the plan in absence of a patient. If the MLC leaf positions show large errors or the IMRT dose distribution deviates from the planning dose distribution above pre-set acceptance criteria, film and ion chamber measurements can be used for further dosimetric investigation.

MC for IMRT Verification Using EPIDs

For a given radiation fluence, MC allows direct modeling of detector responses. This property can be extended to model EPIDs, since they are used for both pretreatment IMRT fluence verification and during treatment dose validation (Chang et al. 2001; McCurdy, Luchka, and Pistorius 2001; Warkentin et al. 2003; Siebers et al. 2004; Van Esch, Depuydt, and Huyskens 2004; Vieira et al. 2004).

Commercial amorphous-silicon (aSi) EPIDs contain high-Z scintillation screens [e.g., the Lanex Fast B screen (Kodak, Rochester, NY)] and are highly sensitive to low-energy photons. As a result, the energy dependence response of aSi EPIDs is substantially different from that of an ionization chamber embedded in a water phantom, and dosimetric EPID measurements differ from those that would be measured in a water phantom (El-Mohri et al. 1999). Accurate prediction of measured EPID images or deconvolution of incident fluence from measured EPID images requires accounting for the detector energy dependence. By directly simulating the detector response on a particle-by-particle basis, MC allows direct incorporation of the detector energy dependence as functions of off-axis distance, MLC beam hardening, and patient scatter. Figure 6 compares measured and MC-computed EPID images for an IMRT field pretreatment IMRT dose verification. The high resolution of the EPID image, along with the high accuracy of the MC-computed images, indicates that EPID-based IMRT dosimetry is well suited for IMRT QA when an MC is used for the IMRT patient dose calculation.

MC in IMRT Plan Optimization

Using MC only as a QA test for post-optimization plan verification allows MC to detect dose-prediction errors (DPEs). However, other than scaling of per-beam MUs for DMLC delivery or per-segment beam weights for SMLC delivery, MC does not correct for the optimization convergence errors (OCEs), which result from inaccuracies in the dose-evaluation algorithms used during plan optimization. Due to inaccurate beamlet dose distributions, the "optimal" solution produced by the inverse-planning optimizer differs from the optimal solution created with accurate beamlets (Ma et al. 2000a; Pawlicki and Ma 2001; Jeraj, Keall, and Siebers 2002). The optimization algorithm can only account for known dose deficiencies during plan optimization. Since the optimization is a balance between target coverage and normal tissue sparing, inaccurate optimization dose evaluation can result in an imbalance of these constraints. When using an accurate algorithm during plan optimization, the intensities of the different IMRT beams from different directions are used to compensate for the dose excesses and deficiencies otherwise inherent in the less accurate dose algorithm. Optimization convergence errors imply that a better optimization result exists.

Which DPEs and OCEs can be accounted for during MC plan optimization depends on whether the MC method is used for fluence prediction, patient dose calculations, or both during plan optimization. In the sections below, we describe

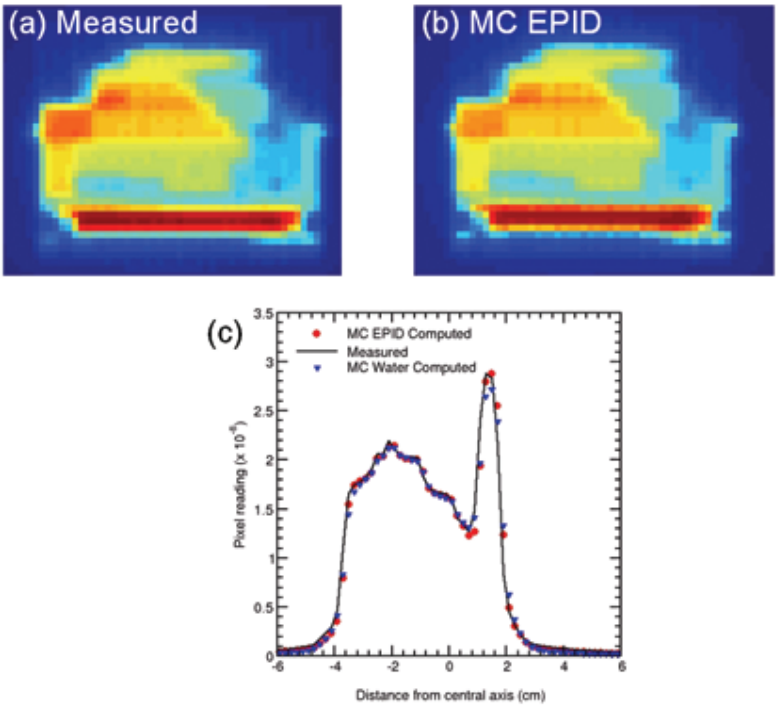

Figure 6. Measured and MC-computed EPID images of a patient IMRT field for pretreatment IMRT dosimetric verification. (a) Measured image; (b) the MC-computed image has $\gamma<1$ for 97% of the points in the image with dose >10% of the maximum. In (c), a profile through the measured and computed images is compared with the dose computed in a water phantom. The MC EPID calculation matches in the intensity peaks and valleys, whereas the MC water phantom calculation deviates in these regions.

approaches used for IMRT plan optimization and consider which residual DPEs and OCEs remain for each method.

Although several TPS vendors indicate that integration of MC into the IMRT optimization process is in the near-term product development, currently no commercial TPSs use MC dose calculations during plan optimization. Therefore, research implementations from noncommercial groups are summarized in what follows. Currently, three groups routinely use MC for IMRT optimization, Fox Chase Cancer Center, University of Tübingen, and Virginia Commonwealth University.

Bixel-based Method

In the bixel-based optimization method, MC is used to precompute individual pencil beams (bixels) through the patient geometry, and the IMRT plan optimization process

determines the weighting of the bixels required to produce the optimal plan (Jeraj and Keall 1999, 2000; Pawlicki and Ma 2001; Shepard et al. 2002; Ma et al. 2003a). By using MC for the patient-transport stage of the dose calculation, the bixel-based method properly accounts for the patient heterogeneities (hence, avoided DPEs due to patient fluence); however, since it does not include the transport through the MLC, DPEs and OCEs may remain due to fluence prediction errors.

The effects of per-bixel MC statistical-uncertainty IMRT dose optimizations have been directly studied for a two-dimensional (2-D) lung tumor example (Table 2). The plan, when optimized using bixels with a 3% 1σ statistical error at D_{max}, showed a 7% underdosage of tumor structures when the dose was reevaluated with a noise-free dose computation (Jeraj and Keall 2000). Even a 0.5% per-bixel statistical dose uncertainty resulted in a 1.2% tumor underdosage, indicating the need for a low per-bixel statistical dose uncertainty for IMRT optimization. The DPEs and OCEs, due to statistical uncertainties, were found to depend upon the objective function used during the optimization.

Jeraj et al. (2002) also used bixels to characterize the DPEs and OCEs due to heterogeneities of SC and PB algorithms for 2-D head-and-neck, prostate, and lung test cases. The DPEs of the algorithms were determined by optimizing with the SC and PB algorithms and comparing resultant dose distributions with an MC recomputation of the SC- and PB-based plans. The OCE was determined by comparison with a plan that used MC during the optimization. Summary results of these DPEs are shown in Table 3. For the SC algorithm, the DPEs were <3%, while for the PB algorithm, they were up to 8% for the lung. The OCEs, in general, were found to be smaller for the SC algorithm than for the PB algorithm, but ranged up to 7% for each algorithm, depending upon the objective function.

Table 2. The Effect of Per-Bixel MC Statistical Uncertainty on Final Plan Quality for a Lung Tumor IMRT Optimization

Bixels, generated with the indicated σ_{stat} dose uncertainty at D_{max}, were used for plan optimization. Following optimization, plans were recomputed using bixels with $\sigma_{stat} \approx 0$, and minimum and maximum target doses were scored. The numbers in parentheses correspond with the doses reported by the optimization. [Adapted from Jeraj and Keall (2000).]

σ_{stat} (%)	Minimum Dose	Maximum Dose
Noise-free	95.0	106.9
0.5	93.8 (95.0)	107.2 (106.9)
1	92.4 (95.0)	107.1 (106.8)
2	91.7 (95.0)	109.0 (106.9)
3	87.0 (94.1)	108.4 (107.0)
4	90.0 (92.5)	109.0 (107.0)

Table 3. Dose-Prediction Errors (DPEs) and Optimization Convergence Errors (OCEs) for Superposition and Pencil Beam Dose Calculations Compared with MC-based Optimization for (a) 2-D Lung, (b) Prostate, and (c) Head-and-Neck Treatment Plans
Values given for the DPE correspond with the mean and standard deviations; while for the OCE, the range of OCEs observed is given. [Adapted from Jeraj, Keall, and Siebers (2002).]

(a)				
	Superposition		Pencil Beam	
Error (%D_{max})	Tumor	Lung	Tumor	Lung
Systematic	–0.1 ± 2	–1 ± 1	+8 ± 3	+6 ± 5
Convergence	2–5	1–4	3–6	6–7
(b)				
	Superposition		Pencil Beam	
	Tumor	Rectum	Tumor	Rectum
Systematic	–0.3 ± 2	–1 ± 1	+5 ± 1	+6 ± 1
Convergence	2–5	2–7	3–6	2–5
(c)				
	Superposition		Pencil Beam	
	Tumor	Spinal cord	Tumor	Spinal Cord
Systematic	–1 ± 2	–3 ± 1	–3 ± 2	+2 ± 1
Convergence	3–6	1–3	3–4	1–3

Three-dimensional MC bixel-based optimization includes the direct aperture optimization (DAO) method described by Shepard et al. (2002). During DAO, MC precomputed 1×0.5 cm^2 bixel weights are optimized, subject to the constraint that they create apertures formed by the MLC. While the DAO process does not include the effects of MLC leakage and scatter radiation, the impact of this DPE is avoided by MC recomputation of the final optimized result, including the MLC sequences used for final beam delivery. Unfortunately, the size of the DPE, caused by neglect of MLC leakage and scatter during optimization, was not reported, nor were comparisons with DAO performed with non-MC dose algorithms.

Field-based IMRT Optimization

In bixel-based dose optimization (above), MC dose computation is performed only once for an entire optimization process. However, for many inverse-planning implementations, dose is recomputed in each optimization iteration or frequently during the optimization process. This allows higher resolution than would be permitted in bixel-based optimization, since there is no need to store dose distributions from each

individual beamlet, as well as direct inclusion of MLC leaf sequences (and MC transport through those sequences) during IMRT optimization. However, this recomputation process amplifies the time-consuming process of MC dose computation. As a result, this section describes techniques used to reduce dose-evaluation time for MC-based inverse planning.

For most optimization algorithms, the number of iterations required to converge to an optimal solution depends on the quality of the initial guess provided to the optimizer. In other words, for IMRT optimization, if the initial fluence estimates are close to the optimal ones, only a few iterations will be required for the optimizer to converge. When pre-optimization with a fast algorithm is used, the MC optimization iterations must only correct for the DPEs and OCEs inherent in the pre-optimization methods.

The Tübingen-developed Hyperion system uses a PB for pre-optimization of the fluences (Laub et al. 2000; Fippel and Nusslin 2003). The PB-derived fluences are used as input to the XVMC algorithm to evaluate the IMRT plan-objective function. Fluence gradients, determined from the PB algorithm, are then used to update the fluence estimates. To efficiently perform the next MC iteration, the first MC is used as a baseline dose computation with fluence increases handled by transporting additional positive weight particles and fluence decreases handled by transporting particles with negative statistical weight (Fippel and Nusslin 2003). When MLC transport is included in the negative weight particle method, the MC source sampling must be identical for successive particles transported in two successive iterations. Source particles affected by the fluence modifications in successive iterations are then run with the particle with both negative and positive beam weights. The negative weight particle method is efficient for small fluence modifications, but becomes more time-consuming than direct simulation when fluence modifications are large.

Even without using negative particle weights, fast dose computations can enhance MC IMRT optimization efficiency. A clinical example can be demonstrated comparing three different optimization methods, with results shown in Figure 7 (isodoses) and

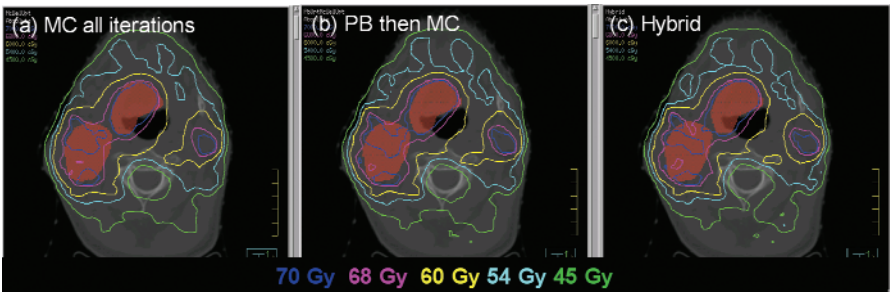

Figure 7. Isodose comparisons for a head-and-neck IMRT plan optimized using three different dose-calculation strategies during optimization. In (a), MC is used for all optimizations. In (b), pre-optimization with a fast PB algorithm is used prior to MC optimization. In (c), the hybrid method is used during optimization.

Figure 8 [dose-volume hostograms (DVHs)]. The first optimization method utilizes MC dose calculation for all optimization iterations and requires 18 MC dose computations to converge. The second method uses PB for pre-optimization, followed by MC-based optimization for 11 iterations before convergence. The third method uses a corrective hybrid-method outlined in Figure 9 (Siebers et al. 2003c). With this method, the majority of the optimization is performed with a fast PB algorithm, but at convergence, MC-based dose distributions are computed, and beam-specific PB correction factors are derived for future optimization iterations. For the case shown in Figure 7 and Figure 8, only three MC dose computations are required for the corrective-hybrid method to converge. The isodose coverage and number of monitor units is the same for the three optimization methods; however, the hybrid method requires less time to complete the optimization.

The number of MC optimization iterations required during the hybrid method depends upon the DPE (hence OCE) of the fast algorithm. In the limit of using an algorithm without DPEs, only one MC iteration is required to validate the dose distribution. Note, in the MC optimization referred to above, that explicit MLC transport was included in the optimization by way of deliverable-based optimization, thereby correcting for the DPEs and OCEs due to both the fluence prediction and heterogeneities in the pre-optimization step.

MC in Intensity-Modulated Electron Beam Optimization

Because of the rapid depth-dose falloff, electron beams are well suited to the treatment of shallow targets while providing the ability to spare distal structures. Energy and

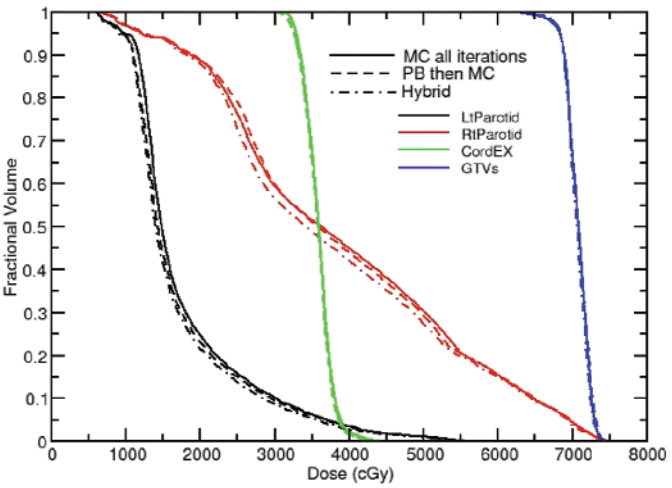

Figure 8. Dose-volume histogram comparison for a head-and-neck IMRT plan optimized using the three different dose-calculation strategies during optimization.

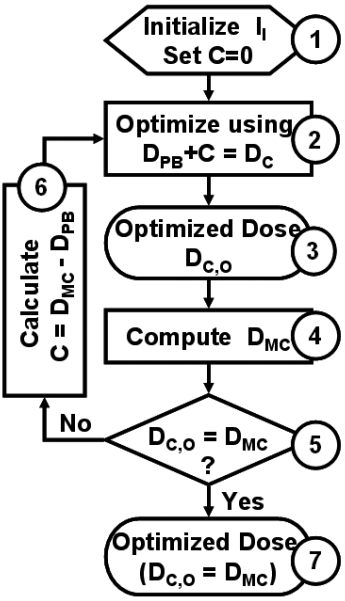

Figure 9. A corrective-based hybrid method for use in IMRT plan optimization. The fluence optimization iterations are performed using a fast pencil beam (PB) algorithm corrected by a Monte Carlo (MC)-derived correction matrix (box 6). Convergence is indicated when the PB-corrected dose is equal to the MC computed dose.

intensity-modulated electron radiation therapy (MERT) has garnered growing interest in recent years (Leavitt, Stewart, and Earley 1990; Hyodynmaa, Gustafsson, and Brahme 1996; Lief, Larsson, and Humm 1996; Zackrisson and Karlsson 1996; Asell et al. 1997; Karlsson, Karlsson, and Ma 1999; Ma et al. 2000b; Lee et al. 2001; Hogstrom et al. 2003). In the optimization process of MERT, lateral dose conformity is achieved by intensity modulation; while along the beam direction, it is achieved by modulating electron incident energy and making use of the sharp dose falloff feature. Using MERT, uniform coverage of the breast and selected portions of the chest wall are possible, while delivering only a low dose to the lung and completely sparing the contralateral breast (Lee, Jiang, and Ma 2000; Ma et al. 2000b, 2003a; Lee et al. 2001; Xiong et al. 2004). MC has played an important role in the development and clinical implementation of MERT.

MC Dose Calculation for MERT

Accurate beamlet dose calculation is important to the MERT treatment-planning optimization process. It has been shown that the electron beam dose distributions calculated by the PB algorithm, as implemented in most commercial TPSs, can be fairly uncertain in the regions near material interfaces and inhomogeneities (Shortt et al. 1986;

Cygler et al. 1987; Mackie et al. 1994; Ma et al. 1999). Figure 10 shows the beamlet dose distributions calculated using the 3-D PB as implemented in a commercial TPS and using MC simulations (Ma et al. 2000b). The dose distributions are for a 1 cm × 1 cm 12-MeV beamlet incident on a patient phantom built from CT data. For beamlets with normal incidence and a 10-cm air gap (figures on top), the difference in the dose distributions on the skin surface and in the heart is evident: the MC-calculated isodose lines vary with the heart contour, while the PB isodose lines remain symmetrical despite the change in material densities. The beamlet distributions again differ significantly in the lung for oblique incidence (bottom figures). The axis of the beamlet is intentionally placed to go through soft tissues and bones. The PB isodose lines seem to stretch according to the beam-axis path length and show no signs of electron build-down near the low-density material. If such inaccurate beamlet distributions are used in the inverse-planning process, one can expect that the resulting treatment plans will be compromised.

Compared to the effect of photon scattering from MLC leaves on the IMRT dose distributions, electron dose distributions are more severely affected by electrons scattered by the collimators and in the intervening air between the treatment head and the patient surface. Shown in Figure 11 are the MC-calculated fluence profiles of 6-, 12-

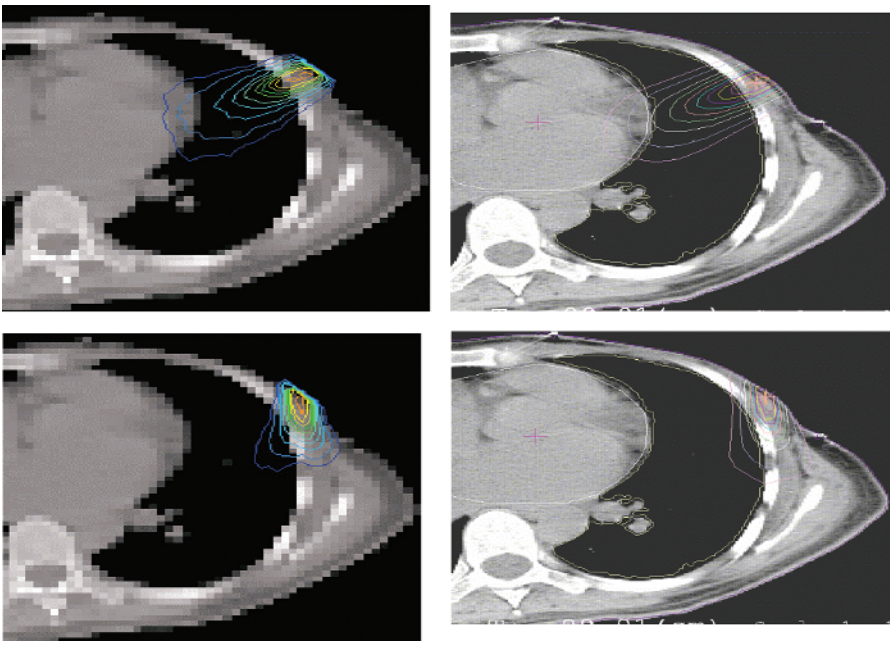

Figure 10. Beamlet dose distributions calculated by Monte Carlo (on the left) and the FOCUS system (on the right). (Adapted from *Phys Med Biol*, vol 45, "Energy- and intensity-modulated electron beams for radiotherapy," C.-M. Ma, T. Pawlicki, M. C. Lee, S. B. Jiang, J. S. Li, J. Deng, B. Yi, E. Mok, and A. L. Boyer, pp. 2293–2311.

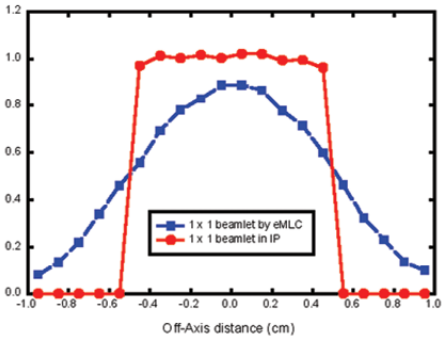

(a)

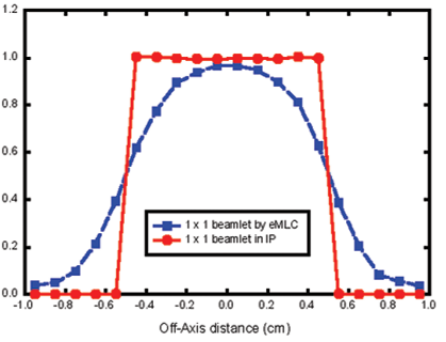

(b)

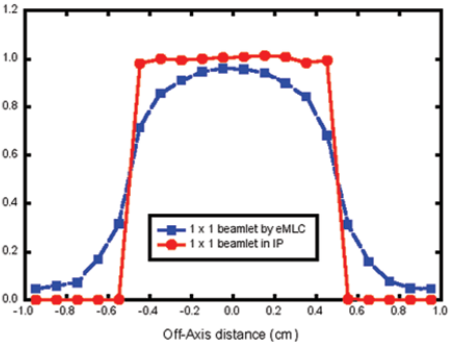

(c)

Figure 11. Comparison of 1 cm × 1 cm beamlet fluence profiles collimated by eMLC with ideal beamlet profiles assumed in the inverse-planning (IP) process. The profiles were obtained at a source-to-surface distance of 100 cm for 6 MeV (a), 12 MeV (b) and 20 MeV (c) electron beams. (Adapted from *Med Phys*, vol 29, "A Monte Carlo investigation of fluence profiles collimated by an electron specific MLC during beam delivery for modulated electron radiation therapy," J. Deng, M. C. Lee, and C.-M. Ma, pp. 2472–2483.

and 20-MeV electron beams collimated by an electron-specific MLC (eMLC) located at the level of the last scraper of the electron applicator. The fluence profiles are severely distorted when 1 cm × 1 cm beamlets are delivered. The fluence profiles extend into the neighboring regions, making the intensities of neighboring regions larger and its own intensity smaller. Therefore, the actual dose distribution delivered by an eMLC can be significantly different from the planned dose distribution, based on virtual beams (Ma et al. 2000b; Deng, Lee, and Ma 2002). Therefore, MC simulations are necessary for both pre- and post-optimization dose calculations for MERT treatment planning.

MC Simulation of MERT Beam Delivery Systems

Different methods have been investigated to deliver intensity-modulated electron fields for MERT. Traditionally, electron beams are shaped using a cutout (or blocks) and beam penetration or range may be modified using a bolus (Low et al. 1992; Klein, Li, and Low 1996). However, it is time consuming to make such beam modifiers and the treatment time would be significantly increased if the beam modifiers used for MERT required many electron beam segments. Both eMLCs and commonly used photon MLCs (pMLC) have been investigated for MERT beam delivery (Leavitt, Stewart, and Earley 1990; Karlsson, Karlsson, and Ma 1999; Lee, Jiang, and Ma 2000; Ma et al. 2000b; McNeeley et al. 2002; Hogstrom et al. 2003). Extensive MC simulations were carried out for electron fields collimated by 1-cm–wide leaves to study the effect of material type and leaf thickness (Lee, Jiang, and Ma 2000; Ma et al. 2000b; Lee et al. 2001). Although the beam penumbral widths did not change significantly for leaf thicknesses smaller than 2 cm, the beam intensity outside the field was affected by the leaf thickness and the atomic number of the leaf material. For a 20-MeV electron beam, 1.5-cm–thick zinc leaves reduced the electron fluence outside the field to about 5% of the central axis value. These electrons were mainly generated by the bremsstrahlung photons in the MLC leaves; 1.5-cm zinc MLC leaves resulted in about a 60% higher photon fluence outside the field, compared with the central axis photon fluence. Some electrons were also scattered off the leaf ends and by air. For 1.5-cm copper, 1.5-cm lead, and 2-cm steel, the electron fluence was about 2.5% of the central axis value. The electron fluence was reduced to about 1.5% if the leaves were made of 1.5-cm tungsten. If the tungsten leaf thickness is increased to 2 cm, the electron fluence will be reduced to less than 1% of the central axis value, and the photon leakage can be reduced to about 50% of the central axis value. The overall effect of the leaf leakage, leaf scattering, air scattering, and the extended source on an electron beam has been studied using MC simulations for an eMLC with 1.5-cm–thick tungsten leaves (Lee, Jiang, and Ma 2000; Ma et al. 2000b; Lee et al. 2001).

MC simulations have been performed for electron beam collimation using a pMLC (Karlsson, Karlsson, and Ma 1999; Lee, Jiang, and Ma 2000). Several modifications to the design of a Varian Clinac 2300CD accelerator have been investigated (Karlsson, Karlsson, and Ma 1999); one modification was to replace the intervening air with helium. This could significantly reduce the effect of electron scattering in the air on the beam penumbra. To solve this problem, the patient has to be brought closer to the

MLC to reduce the air scattering effect. Rounded pMLC leaf ends could scatter the electrons very significantly to degrade the beam characteristics near the field edges. Focused leaf ends could greatly improve the beam edges and provided even slightly better dose profiles inside the field for a 20-MeV electron beam, compared with an eMLC, primarily due to the reduction of electron scattering in the accelerator head (helium vs. air). The dose outside the field was slightly lower for the electron MLC than for the pMLC. For a 6-MeV beam, an electron MLC gave slightly better surface dose profiles both inside and outside the field than the focused and unfocused photon MLC (not shown). The difference in the dose profiles decreases with depth. It is evident that an eMLC will have dosimetric characteristics similar to those of a pMLC with focused leaf ends, but without the need to replace the air in the accelerator head with helium (Lee, Jiang, and Ma 2000; Ma et al. 2000b; Lee et al. 2001).

Case Studies on MERT and Mixed Beam Therapy

MC investigations have been carried out on the efficacy of MERT and other treatment techniques for breast treatment (Lee, Jiang, and Ma 2000; Ma et al. 2000b, 2003a; Lee et al. 2001; Xiong et al. 2004). The same MC dose-calculation and plan-optimization software was used to compare different treatment techniques. Figure 12 compares dose distributions from MERT, tangential IMRT, and conventional wedged beams. The breast patient had a relatively large target volume with significant volumes of lung and heart in the tangential beams due to the curved chest-wall anatomy. The target dose was improved with intensity-modulated tangents, since the target dose homogeneity was the only goal for the optimization. However, this was achieved at the cost of the lung and heart doses; both the lung and heart doses were increased slightly to improve the target dose through the thicker portion of the breast. On the other hand, the MERT plan had about 10% dose heterogeneity in the target volume, while the lung and heart doses were much improved compared with the photon

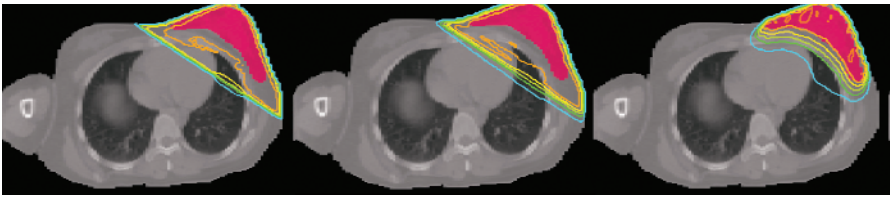

(a) **(b)** **(c)**

Figure 12. Isodose distributions planned using wedged tangential photon beams (a), intensity-modulated tangential beams (b). and four-field MERT (d). The 55-, 50-, 40-, 30-, 20- and 10-Gy isodose lines are shown. (Adapted from *Phys Med Biol*, vol 48, "A comparative dosimetric study on tangential photon beams, intensity-modulated radiation therapy (IMRT) and modulated electron radiotherapy (MERT) for breast cancer treatment," C.-M. Ma, M. Ding, J. S. Li, M. C. Lee, T. Pawlicki, and J. Deng, pp. 909–924. © 2003, with permission from IOP Publishing.)

beams. The maximum lung dose was under 20 Gy, and the maximum heart dose was under 15 Gy, compared with about 50 Gy for both photon plans. This was achieved by exposing low-energy beams to the peripheral regions and higher-energy beams in the central, thick portion of the target volume.

Fox Chase Cancer Center was the first to implement MC treatment planning for the treatment of breast cancer using tangential IMRT (Li et al. 2004) and later using hypofractionated radiotherapy incorporating IMRT and a concurrent electron boost (Freedman et al. 2006). Patients received 20 treatment fractions during the treatment course with 2.8 Gy/fraction to the tumor bed and 2.25 Gy/fraction to the rest of the breast. Accurate MC dose calculation and the combination of IMRT and MERT ensured homogeneous and conformal target coverage. Xiong et al. (2004) showed that dose inhomogeneity can be reduced significantly (by 20%) by optimizing tangential IMRT and modulated electron beams. Figure 13 shows that the tumor bed receives more conformal dose distribution from combined IMRT and MERT optimization, compared with simply adding an electron boost field or optimizing IMRT based on a given electron boost field. Intensity modulation of photon and electron beams may provide a significant reduction in the peak lung dose compared with IMRT or conventional photons, followed by an independent boost electron field. This treatment technique shows significant promise for breast cancer treatment and is under development for other treatment sites.

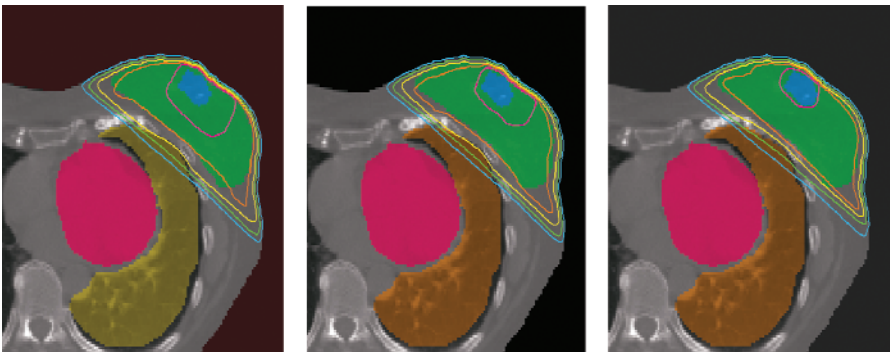

(a) **(b)** **(c)**

Figure 13. Isodose distributions of hypofractionated breast treatment: (a) optimizing IMRT based on an existing electron field; (b) optimizing IMRT and the weight of the electron field; and (c) optimizing both IMRT and MERT to achieve the best dose conformity. (Adapted from *Phys Med Biol*, vol 49, "Optimization of combined electron and photon beams for breast cancer," W. Xiong, J. Li, L. Chen, R. A. Price, G. Freedman, M. Ding, L. Qin, J. Yang, and C.-M. Ma, pp. 1973–1989. © 2004, with permission from IOP Publishing.)

References

American Association of Physicists in Medicine (AAPM). (1983). "A protocol for the determination of absorbed dose from high-energy photon and electron beams." *Med Phys* 10(6):741–771.

Aaronson, R. F., J. J. DeMarco, I. J. Chetty, and T. D. Solberg. (2002). "A Monte Carlo based phase space model for quality assurance of intensity modulated radiotherapy incorporating leaf specific characteristics." *Med Phys* 29(12):2952–2958.

Alber, M., M. Birkner, A. Bakai, O. Dohm, M. Fippel, F. Paulsen, C. Belka, W. Budach, and F. Nüsslin. 2003. Routine use of Monte Carlo dose computation for head and neck IMRT optimization." *Int J Radiat Oncol Biol Phys* 57(Suppl):S208 (Abstract).

Arnfield, M. R., C. H. Siantar, J. Siebers, P. Garmon, L. Cox, and R. Mohan. (2000). "The impact of electron transport on the accuracy of computed dose." *Med Phys* 27(6):1266–1274.

Åsell, M., S. Hyodynmaa, A. Gustafsson, and A. Brahme. (1997). "Optimization of 3D conformal electron beam therapy in inhomogeneous media by concomitant fluence and energy modulation." *Phys Med Biol* 42(11):2083–2100.

Boudreau, C., E. Heath, J. Seuntjens, O. Ballivy, and W. Parker. (2005). "IMRT head and neck treatment planning with a commercially available Monte Carlo based planning system." *Phys Med Biol* 50(5):879–890.

Boyer, A. L., and J. P. Strait. "Delivery of Intensity-Modulated Treatments with Dynamic Multileaf Collimator" in *Proceedings of the XIIth International Conference on the Use of Computers in Radiation Therapy* (*XIIth ICCR*). D. D. Leavitt and G. Starkschall (Eds.). Salt Lake City, UT, May 37–30, 1997. Madison, WI: Medical Physics Publishing, pp. 13–15, 1997.

Boyer, A., L. Xing, C.-M. Ma, B. Curran, R. Hill, A. Kania, and A. Bleier. (1999). "Theoretical considerations of monitor unit calculations for intensity modulated beam treatment planning." *Med Phys* 26(2):187–195.

Boyer, A. L., E. B. Butler, T. A. DiPetrillo, M. J. Engler, B. Fraass, W. Grant III, C. C. Ling, D. A. Low, T. R. Mackie, R. Mohan, J. A. Purdy, M. Roach, J. G. Rosenman, L. J. Verhey, J. W. Wong, R. L. Cumberlin, H. Stone, and J. R. Palta. (2001). "Intensity-modulated radiotherapy: Current status and issues of interest." *Int J Radiat Oncol Biol Phys* 51(4):880–914.

Brahme, A. (1988). "Optimization of stationary and moving beam radiation therapy techniques." *Radiother Oncol* 12(2):129–140.

Briesmeister, J. F. A General Monte Carlo N–Particle Transport Code, Version 4C, Technical Report No LA-13709-M. Los Alamos National Laboratory, 2000.

CERN Application Software Group, and Computing and Network Division. GEANT-Detector Description and Simulation Tool. CERN Program Library Long Writeup W5013. Geneva, Switzerland: CERN, 1995.

Chang, J., G. S. Mageras, C. C. Ling, and W. Lutz. (2001). "An iterative EPID calibration procedure for dosimetric verification that considers the EPID scattering factor." *Med Phys* 28(11):2247–2257.

Chui, C. S., T. LoSasso, and S. Spirou. (1994). "Dose calculation for photon beams with intensity modulation generated by dynamic jaw or multileaf collimations." *Med Phys* 21(8):1237–1244.

Convery, D. J., and M. E. Rosenbloom. (1992). "The generation of intensity-modulated fields for conformal radiotherapy by dynamic collimation." *Phys Med Biol* 37:1350–1374.

Cygler, J., J. J. Battista, J. W. Scrimger, E. Mah, and J. Antolak. (1987). "Electron dose distributions in experimental phantoms: A comparison with 2D pencil beam calculations." *Phys Med Biol* 32(9):1073–1086.

De Vlamynck, K., H. Palmans, F. Verhaegen, C. De Wagter, W. De Neve, and H. Thierens. (1999). "Dose measurements compared with Monte Carlo simulations of narrow 6 MV multileaf collimator shaped photon beams." *Med Phys* 26(9):1874–1882.

Deng, J., M. C. Lee, and C.-M. Ma. (2002). "A Monte Carlo investigation of fluence profiles collimated by an electron specific MLC during beam delivery for modulated electron radiation therapy." *Med Phys* 29(11):2472–2483.

Deng, J., T. Pawlicki, Y. Chen, J. Li, S. B. Jiang, and C.-M. Ma. (2001). "The MLC tongue-and-groove effect on IMRT dose distributions." *Phys Med Biol* 46(4):1039–1060.

El-Mohri, Y., L. E. Antonuk, J. Yorkston, K. W. Jee, M. Maolinbay, K. L. Lam, and J. H. Siewerdsen. (1999). "Relative dosimetry using active matrix flat-panel imager (AMFPI) technology." *Med Phys* 26(8):1530–1541.

Ezzell, G. A., J. M. Galvin, D. Low, J. R. Palta, I. Rosen, M. B. Sharpe, P. Xia, Y. Xiao, L. Xing, and C. X. Yu. (2003). "Guidance document on delivery, treatment planning, and clinical implementation of IMRT: Report of the IMRT Subcommittee of the AAPM Radiation Therapy Committee." *Med Phys* 30(8):2089–2115.

Fan, J., J. Li, L. Chen, S. Stathakis, W. Luo, F. du Plessis, W Xiong, and C.-M. Ma. (2006). "A practical Monte Carlo MU verification tool for IMRT quality assurance." *Phys Med Biol* (In press).

Fippel, M., and F. Nüsslin. (2003). "Smoothing Monte Carlo calculated dose distributions by iterative reduction of noise." *Phys Med Biol* 48(10):1289–1304.

Fix, M. K., P. Manser, E. J. Born, R. Mini, and P. Ruegsegger. (2001). "Monte Carlo simulation of a dynamic MLC based on a multiple source model." *Phys Med Biol* 46 (12):3241-57.

Freedman, G. M., P. R. Anderson, L. G. Goldstein, J. Li, C.-M. Ma, A. Hanlon, D. Watkins-Bruner, N. Nicolaou, M. Torosian, E. Sigurdson, J. Hoffman, N. Joseph, and M. Morrow. (2006). "Initial findings from a four-week course of radiation for breast cancer using hypofractionated intensity modulated radiation therapy (IMRT) with an incorporated boost." *Int J Radiat Oncol Biol Phys* (Submitted).

Hartmann Siantar, C. L., R. S. Walling, T. P. Daly, B. Faddegon, N. Albright, P. Bergstrom, A. F. Bielajew, C. Chuang, D. Garrett, R. K. House, D. Knapp, D. J. Wieczorek, and L. J. Verhey. (2001). "Description and dosimetric verification of the PEREGRINE Monte Carlo dose calculation system for photon beams incident on a water phantom." *Med Phys* 28(7):1322–1337.

Heath, E., and J. Seuntjens. (2003). "Development and validation of a BEAMnrc component module for accurate Monte Carlo modelling of the Varian dynamic Millennium multileaf collimator." *Phys Med Biol* 48(24):4045–4063.

Heath, E., J. Seuntjens, and D. Sheikh-Bagheri. (2004). "Dosimetric evaluation of the clinical implementation of the first commercial IMRT Monte Carlo treatment planning system at 6 MV." *Med Phys* 31(10):2771–2779.

Hogstrom, K. R., J. A. Antolak, R. J. Kudchadker, C.-M. Ma, and D. D. Leavitt. "Modulated Electron Therapy" in *Intensity-Modulated Radiation Therapy: The State of the Art*. T. R. Mackie and J. R. Palta (Eds.). Proceedings of the 2003 AAPM Summer School. Madison, WI: Medical Physics Publishing, pp. 749–786, 2003.

Hounsell, A. R. (1998). "Monitor chamber backscatter for intensity modulated radiation therapy using multileaf collimators." *Phys Med Biol* 43(2):445–454.

Hyodynmaa, S., A. Gustafsson, and A. Brahme. (1996). "Optimization of conformal electron beam therapy using energy- and fluence-modulated beams." *Med Phys* 23(5):659–666.

Ibbott, G., A. Nelson, D. Followill, P. Balter, and W. F. Hanson. "An Anthropomorphic Head and Neck Phantom for the Evaluation of Intensity Modulated Radiation Therapy" in *Standards and Codes of Practice in Medical Radiation Dosimetry.* IAEA-CA-96-122. Vienna, Austria: IAEA, pp. 209–217, 2002.

Jeraj, R., and P. Keall. (1999). "Monte Carlo-based inverse treatment planning." *Phys Med Biol* 44(8):1885–1896.

———. (2000). "The effect of statistical uncertainty on inverse treatment planning based on Monte Carlo dose calculation." *Phys Med Biol* 45(12):3601–3613.

Jeraj, R., P. J. Keall, and J. V. Siebers. (2002). "The effect of dose calculation accuracy on inverse treatment planning." *Phys Med Biol* 47(3):391–407.

Jiang, S. B., A. L. Boyer, and C.-M. Ma. (2001). "Modeling the extrafocal radiation and monitor chamber backscatter for photon beam dose calculation." *Med Phys* 28(1):55–66.

Jones, A. O., and I. J. Das. (2005). "Comparison of inhomogeneity correction algorithms in small photon fields." *Med Phys* 32(3):766–776.

Jones, A. O., I. J. Das, and F. L. Jones, Jr. (2003). "A Monte Carlo study of IMRT beamlets in inhomogeneous media." *Med Phys* 30(3):296–300.

Kapur, A., C.-M. Ma, and A. L. Boyer. (2000). "Monte Carlo simulations for multileaf-collimator leaves: Design and dosimetry." *Med Phys* 27(6):1410.

Karlsson, M. G., M. Karlsson, and C. M. Ma. (1999). "Treatment head design for multileaf collimated high-energy electrons." *Med Phys* 26(10):2161–2167.

Kawrakow, I. (2000). "Accurate condensed history Monte Carlo simulation of electron transport. I. EGSnrc, the new EGS4 version." *Med Phys* 27(3):485–498.

Keall, P. J., J. V. Siebers, M. Arnfield, J. O. Kim, and R. Mohan. (2001). "Monte Carlo dose calculations for dynamic IMRT treatments." *Phys Med Biol* 46(4):929–941.

Kim, J. O., J. V. Siebers, P. J. Keall, M. R. Arnfield, and R. Mohan. (2001). "A Monte Carlo study of radiation transport through multileaf collimators." *Med Phys* 28(12):2497–2506.

Klein, E. E., Z. Li, and D. A. Low. (1996). "Feasibility study of multileaf collimated electrons with a scattering foil based accelerator." *Radiother Oncol* 46:189–196.

Laub, W., M. Alber, M. Birkner, and F. Nüsslin. (2000). "Monte Carlo dose computation for IMRT optimization." *Phys Med Biol* 45(7):1741–1754.

Leal, A., F. Sanchez-Doblado, R. Arrans, J. Rosello, E. C. Pavon, and J. I. Lagares. (2003). "Routine IMRT verification by means of an automated Monte Carlo simulation system." *Int J Radiat Oncol Biol Phys* 56(1):58–68.

Leavitt, D. D., J. R. Stewart, and L. Earley. (1990). "Improved dose homogeneity in electron arc therapy achieved by a multiple-energy technique." *Int J Radiat Oncol Biol Phys* 19:159–165.

Lee, M. C. (2002). Monte Carlo Simulations of Dynamic MLC Beam Delivery for IMRT. Ph.D. Thesis. Stanford University, Stanford, CA.

Lee, M. C., S. B. Jiang, and C.-M. Ma. (2000). "Monte Carlo and experimental investigations of multileaf collimated electron beams for modulated electron radiation therapy." *Med Phys* 27(12):2708–2718.

Lee, M. C., J. Deng, J. Li, S. B. Jiang, and C.-M. Ma. (2001). "Monte Carlo based treatment planning for modulated electron beam radiation therapy." *Phys Med Biol* 46(8):2177–2199.

Li, J. S., G. M. Freedman, R. Price, L. Wang, P. Anderson, L. Chen, W. Xiong, J. Yang, A. Pollack, and C.-M. Ma. (2004). "Clinical implementation of intensity-modulated tangential beam irradiation for breast cancer." *Med Phys* 31(5):1023–1031.

Li, X. A., L. Ma, C. X. Yu, S. Naqvi, and T. Holmes. (2000). "Monte Carlo dose verification for intensity modulated arc therapy." *Int J Radiat Oncol Biol Phys* 48(3S):216.

Li, X. A., L. Ma, S. Naqvi, R. Shih, and C. Yu. (2001). "Monte Carlo dose verification for intensity-modulated arc therapy." *Phys Med Biol* 46(9):2269–2282.

Lief, E. P., A. Larsson, and J. L. Humm. (1996). "Electron dose profile shaping by modulation of a scanning elementary beam." *Med Phys* 23(1):33–44.

Liu, H. H., F. Verhaegen, and L. Dong. (2001). "A method of simulating dynamic multileaf collimators using Monte Carlo techniques for intensity-modulated radiation therapy." *Phys Med Biol* 46(9):2283–2298.

Low, D. A., G. S. Starkshall, W. Bujnowsli, L. L. Wang, and K. R. Hogstrom. (1992). "Electron bolus design for radiotherapy treatment planning: Bolus design algorithms." *Med Phys* 19:115–24.

Luo, W., J. Li, R. Price, L. Chen, J. Yang, J. Fan, Z. Chen, S. McNeeley, and C.-M. Ma. (2006). "Monte Carlo based IMRT QA using MLC log files and R/V outputs." *Med Phys* (Conditionally accepted).

Ma, C.-M., E. Mok, A. Kapur, T. Pawlicki, D. Findley, S. Brain, K. Forster, and A. L. Boyer. (1999). "Clinical implementation of a Monte Carlo treatment planning system." *Med Phys* 26(10):2133–2143.

Ma, C.-M., T. Pawlicki, S. B. Jiang, J. S. Li, J. Deng, E. Mok, A. Kapur, L. Xing, L. Ma, and A. L. Boyer. (2000a). "Monte Carlo verification of IMRT dose distributions from a commercial treatment planning optimization system." *Phys Med Biol* 45(9):2483–2495.

Ma, C.-M., T. Pawlicki, M. C. Lee, S. B. Jiang, J. S. Li, J. Deng, B. Yi, E. Mok, and A. L. Boyer. (2000b). "Energy- and intensity-modulated electron beams for radiotherapy." *Phys Med Biol* 45(8):2293–2311.

Ma, C.-M., M. Ding, J. S. Li, M. C. Lee, T. Pawlicki, and J. Deng. (2003a). "A comparative dosimetric study on tangential photon beams, intensity-modulated radiation therapy (IMRT) and modulated electron radiotherapy (MERT) for breast cancer treatment." *Phys Med Biol* 48(7):909–924.

Ma, C.-M., S. B. Jiang, T. Pawlicki, Y. Chen, J. S. Li, J. Deng, and A. L. Boyer. (2003b). "A quality assurance phantom for IMRT dose verification." *Phys Med Biol* 48(5):561–572.

Ma, C.-M., R. A. Price, Jr., J. S. Li, L. Chen, L. Wang, E. Fourkal, L. Qin, and J. Yang. (2004). "Monitor unit calculation for Monte Carlo treatment planning." *Phys Med Biol* 49(9):1671–1687.

Mackie, T. R., and J. R. Palta (Eds.). *Intensity-Modulated Radiation Therapy: The State of the Art*. Madison, WI: Medical Physics Publishing, 2003.

Mackie, T. R., J. Deasy, T. Holmes, and J. Fowler. (1994). "Optimization of radiation therapy and the development of multi-leaf collimation." *Int J Radiat Oncol Biol Phys* 28:784–785.

McCurdy, B. M., K. Luchka, and S. Pistorius. (2001). "Dosimetric investigation and portal dose image prediction using an amorphous silicon electronic portal imaging device." *Med Phys* 28(6):911–924.

McNeeley, S., J. Li, R. Price, L. Chen, M. Ding, E. Fourkal, and C.-M. Ma. (2002). "An electron specific multileaf collimator for modulated electron radiation therapy." *Med Phys* 28:1286.

Mihaylov, I., F. Lerma, M. Fatyga, and J. Siebers. (2006). "Quantification of the impact of fluence prediction and tissue heterogeneities on dynamic IMRT dose calculations." *Med Phys* (Submitted and 2005 Abstract).

Mohan, R., M. Arnfield, S. Tong, Q. Wu, and J. Siebers. (2000). "The impact of fluctuations in intensity patterns on the number of monitor units and the quality and accuracy of intensity modulated radiotherapy." *Med Phys* 27(6):1226–1237.

Nelson, R., H. Hirayama, and D. W. O. Rogers. "The EGS4 Code System" in *Stanford Linear Accelerator Center Report*. Stanford, CA: Stanford University, 1985.

Pawlicki, T., and C.-M. Ma. (2001). "Monte Carlo simulation for MLC-based intensity-modulated radiotherapy." *Med Dosim* 26(2):157–168.

Pawlicki, T., G. Luxton, Q. T. Le, D. Findley, and C.-M. Ma. (2004). "Lens dose in MLC-based IMRT treatments of the head and neck." *Int J Radiat Oncol Biol Phys* 59(1):293–299.

Reynaert, N., M. Coghe, B. De Smedt, L. Paelinck, B. Vanderstraeten, W. De Gersem, B. Van Duyse, C. De Wagter, W. De Neve, and H. Thierens. (2005). "The importance of accurate linear accelerator head modelling for IMRT Monte Carlo calculations." *Phys Med Biol* 50(5):831–846.

Rogers, D. W. O., B. A. Faddegon, G. X. Ding, C.-M. Ma, J. We, and T. R. Mackie. (1995). "BEAM: A Monte Carlo code to simulate radiotherapy units." *Med Phys* 22(5):503–524.

Rogers, D. W.O., C.-M. Ma, G. X. Ding, B. R. Walters, D. Sheikh-Bagheri, and G. G. Zhang. *BEAMnrc Users Manual*. Ottawa, Canada: National Research Council, 2001.

Seco, J., E. Adams, M. Bidmead, M. Partridge, and F. Verhaegen. (2005). "Head-and-neck IMRT treatments assessed with a Monte Carlo dose calculation engine." *Phys Med Biol* 50(5):817–830.

Shepard, D. M., M. A. Earl, X. A. Li, S. Naqvi, and C. Yu. (2002). "Direct aperture optimization: A turnkey solution for step-and-shoot IMRT." *Med Phys* 29(6):1007–1018.

Shortt, K. R., C. K. Ross, A. F. Bielajew, and D. W. O. Rogers. (1986). "Electron beam dose distributions near standard inhomogeneities." *Phys Med Biol* 31(3):235–249.

Siebers, J., and R. Mohan. "Monte Carlo and IMRT" in *Intensity-Modulated Radiation Therapy: The State of the Art*. T. R. Mackie and J. R. Palta (Eds.). Proceedings of the 2003 AAPM Summer School. Madison, WI: Medical Physics Publishing, pp. 531–560, 2003.

Siebers, J. V., P. J. Keall, J. O. Kim, and R. Mohan. (2002a). "A method for photon beam Monte Carlo multileaf collimator particle transport." *Phys Med Biol* 47(17):3225–3249.

Siebers, J. V., M. Lauterbach, P. J. Keall, and R. Mohan. (2002b). "Incorporating multi-leaf collimator leaf sequencing into iterative IMRT optimization." *Med Phys* 29(6):952–959.

Siebers, J. V., M. Lauterbach, S. Tong, Q. Wu, and R. Mohan. (2002c). "Reducing dose calculation time for accurate iterative IMRT planning." *Med Phys* 29(2):231–237.

Siebers, J. V., J. O. Kim, L. Ko, P. J. Keall, and R. Mohan. (2004). "Monte Carlo computation of dosimetric amorphous silicon electronic portal images." *Med Phys* 31(7):2135–2146.

Van de Walle, J., C. Martens, N. Reynaert, H. Palmans, M. Coghe, W. De Neve, C. De Wagter, and H. Thierens. (2003). "Monte Carlo model of the Elekta SLiplus accelerator: Validation of a new MLC component module in BEAM for a 6 MV beam." *Phys Med Biol* 48(3):371–385.

Van Esch, A., T. Depuydt, and D. P. Huyskens. (2004). "The use of an aSi-based EPID for routine absolute dosimetric pre-treatment verification of dynamic IMRT fields." *Radiother Oncol* 71(2):223–234.

Verhaegen, F., R. Symonds-Tayler, H. H. Liu, and A. E. Nahum. (2000). "Backscatter towards the monitor ion chamber in high-energy photon and electron beams: Charge integration versus Monte Carlo simulation." *Phys Med Biol* 45(11):3159–3170.

Vieira, S. C., M. L. Dirkx, B. J. Heijmen, and H. C. de Boer. (2004). "SIFT: A method to verify the IMRT fluence delivered during patient treatment using an electronic portal imaging device." *Int J Radiat Oncol Biol Phys* 60(3):981–993.

Wang, L., E. Yorke, and C. S. Chui. (2002). "Monte Carlo evaluation of 6 MV intensity modulated radiotherapy plans for head and neck and lung treatments." *Med Phys* 29(11):2705–2717.

Wang, X., S. Spirou, T. LoSasso, J. Stein, C. S. Chui, and B. Mohan. (1996). "Dosimetric verification of intensity-modulated fields." *Med Phys* 23(3):317–327.

Warkentin, B., S. Steciw, S. Rathee, and B. G. Fallone. (2003). "Dosimetric IMRT verification with a flat-panel EPID." *Med Phys* 30(12):3143–3155.

Webb, S. *The Physics of Conformal Radiotherapy: Advances in Technology*. Bristol, UK: IOP Publishing, 1997.

Xiong, W., J. Li, L. Chen, R. A. Price, G. Freedman, M. Ding, L. Qin, J. Yang, and C.-M. Ma. (2004). "Optimization of combined electron and photon beams for breast cancer." *Phys Med Biol* 49(10):1973–1989.

Yang, J., J. Li, L. Chen, R. Price, S. McNeeley, L. Qin, L. Wang, W. Xiong, and C.-M. Ma. (2005). "Dosimetric verification of IMRT treatment planning using Monte Carlo simulations for prostate cancer." *Phys Med Biol* 50(5):869–878.

Zackrisson, B., and M. Karlsson. (1996). "Matching of electron beams for conformal therapy of target volumes at moderate depths." *Radiother Oncol* 39:261–270.